Monthly Weather Review

A Scale-Aware Anticipated Potential Vorticity Method on Variable-resolution Meshes

--Manuscript Draft--

Manuscript Number:	
Full Title:	A Scale-Aware Anticipated Potential Vorticity Method on Variable-resolution Meshes
Article Type:	Article
Corresponding Author:	Qingshan Chen, Ph.D Florida State University Tallahassee , FL UNITED STATES
Corresponding Author's Institution:	Florida State University
First Author:	Qingshan Chen, Ph.D
All Authors:	Qingshan Chen, Ph.D
	Max Gunzburger
	Todd Ringler
Abstract:	A scale-aware formulation of the anticipated potential vorticity method (APVM), previously derived for quasi-uniform unstructured grids, is evaluated on multi-resolution grids. Comparison is made to the original, non-scale-aware formulation of APVM. Numerical simulations are performed using the shallow water standard test case \#5. The scale-awareness of the new formulation is demonstrated by the following observations: ({\it i}) the range of optimal values for the single parameter of the new formulation is much more focused than that of the original formulation; ({\it ii}) within the optimal parameter range, the new formulation is able to produce better results in terms of errors in the potential enstrophy spectrum curves; ({\it iii}) in a challenging situation when the contrast ratio between the fine and coarse resolutions is very high, the new formulation is able to maintain proper dissipation in both high- and low-resolution regions, and thus to produce a realistic potential enstrophy spectrum curve; ({\it iv}) the new formulation is robust in that a single optimal parameter obtained for a specific grid can be safely used on other grids as well.
Suggested Reviewers:	

A Scale-Aware Anticipated Potential Vorticity Method on Variable-resolution Meshes

Qingshan Chen *

Florida State University

Max Gunzburger

Florida State University

Todd Ringler

Los Alamos National Laboratory

Corresponding author address: Department of Scientific Computing, Florida State University, Tallahassee, FL 32310.

E-mail:qchen3@fsu.edu

ABSTRACT

A scale-aware formulation of the anticipated potential vorticity method (APVM), previously derived for quasi-uniform unstructured grids, is evaluated on multi-resolution grids. Comparison is made to the original, non-scale-aware formulation of APVM. Numerical simulations are performed using the shallow water standard test case #5. The scale-awareness of the new formulation is demonstrated by the following observations: (*i*) the range of optimal values for the single parameter of the new formulation is much more focused than that of the original formulation; (*ii*) within the optimal parameter range, the new formulation is able to produce better results in terms of errors in the potential enstrophy spectrum curves; (*iii*) in a challenging situation when the contrast ratio between the fine and coarse resolutions is very high, the new formulation is able to maintain proper dissipation in both high- and low-resolution regions, and thus to produce a realistic potential enstrophy spectrum curve; (*iv*) the new formulation is robust in that a single optimal parameter obtained for a specific grid can be safely used on other grids as well.

1. Introduction

Global climate models have become a critical contributor to the study of climate change and the accompanying extreme weather/climate events. To meet the increasing demands on climate modeling, scientists strive to build climate models that are accurate, tractable, and flexible. For example, a new *global-to-regional multi-resolution approach* (Ringler et al. 2008; Ringler et al.) has been proposed for which only a single grid, with variable resolutions and with smooth transitions between fine and coarse grid regions, is involved; see also Chen and Gunzburger.

The long-term success of models operating on multi-resolution grids depends on access to scale-aware subgrid closures that are able to act appropriately across the vast range of scales present in the model. However, developing scale-aware subgrid closures for the ocean and atmosphere has been a difficult and unmet challenge. Whereas closures for clouds in the atmosphere (Arakawa and Schubert 1974) and eddies in the ocean (Gent and McWilliams 1990) have clearly been successful, neither has been generalized across spatial and/or temporal scales.

We endeavor to develop scale-aware subgrid closures for use in the new generation of climate models operating on multi-resolution grids. Given the difficulty in generalizing Arakawa and Schubert (1974) and Gent and McWilliams (1990) across scales, we have chosen to start with the more tractable problem of generalizing a 2-D turbulence closure scheme across scales. Through this simpler, yet relevant, example, we hope to construct a conceptual framework that will allow us to generalize more difficult parameterizations across spatial and temporal scales. As the first step in a series of efforts, we aim to generalize the anticipated potential vorticity method (APVM) of Sadourny and Basdevant (1985) for multi-resolution simulations. The APVM is a subgrid eddy closure scheme that is perfectly energy-conserving and, at the same time, enstrophy-dissipating. In the context of a shallow-water flows, the

APVM can be described by

$$\frac{\partial \mathbf{u}}{\partial t} + (q - D)\mathbf{k} \times h\mathbf{u} = -\nabla \left(gh + \frac{1}{2}|\mathbf{u}|^2 \right), \tag{1}$$

with $\mathbf{u}$ and gh denoting the velocity and geopotential fields, respectively, $q \equiv (\mathbf{k}\cdot\nabla\times\mathbf{u}+f)/h$ the potential vorticity, D a correction to the potential vorticity q, and $\mathbf{k}$ the unit vector in the vertical direction. The modified system remains energy conserving, as the term $\mathbf{k} \times \mathbf{u}$ is perpendicular to the horizontal velocity component. As discussed in detail in Section 2, the term D is chosen so that the modified system dissipates the potential enstrophy, i.e., the variance of the potential vorticity. In its simplest form, we have

$$D = \gamma \mathbf{u} \cdot \nabla q. \tag{2}$$

It was proposed in Sadourny and Basdevant (1985) that[1] γ should be a time-scale-selective parameter and thus should take the form

$$\gamma = \sigma dt, \tag{3}$$

with dt denoting the time step and σ an independent parameter. After substituting (3) into (2), we see that, with $dt\mathbf{u}$ being the displacement vector and ∇q being the change rate of the potential vorticity over space, D represents the variation of the potential vorticity along the the fluid path. As a result, the quantity $q - D$ represents the value of the potential vorticity at an *upstream* point, hence the name *anticipated* potential vorticity method.

Clearly, the primary challenge in the development of any scale-aware parameterization will be the identification of parameter(s) that are largely insensitive to the spatial and temporal resolution of the numerical model. So whereas the form of γ in (3) is appealing because of its physical interpretation, there is no analysis or computational evidence available to support the invariance of the parameter σ when using the APVM; in fact, our experience shows that the optimal value of σ is indeed significantly influenced by the time-step size and

[1] In the foregoing reference, θ instead of γ is used for the APVM coefficient. We have switched to γ to avoid confusion with the spherical coordinante θ introduced later.

the grid resolution of each particular simulation. In our opinion, this puts a severe constraint on the applicability of the form (3) for γ because, for each particular simulation, without extensive fine tuning and comparisons, it is not clear what is the optimal value of σ one should use.

In Chen et al. (2011), a scale-aware formulation of the APVM is derived through a scale analysis technique. The new formulation contains a single parameter that is, in principle, invariant to temporal and spatial scales. The new formulation is tested on quasi-uniform spherical centroidal Voronoi tessellation (SCVT) grids (Du et al. 1999, 2003). In Chen et al. (2011) the authors aim to address the following question: how does the optimal parameter change in response to the changes in the grid resolution of the quasi-uniform grid? Numerical results, using the Model for Prediction Across Scales (MPAS, Ringler et al. (2010)) framework, demonstrate that the optimal parameter is invariant to the time step of the discrete model, and is only weakly dependent on the grid resolution. Even though a strict invariance of the optimal parameter with respect to the grid resolution is not achieved, which we doubt would even be possible, it is shown that the closure is relatively insensitive near the optimal parameter, and therefore a parameter determined on a specific grid can be safely used on other grids.

In this work we aim to extend the scale-aware formulation of the APVM, developed in Chen et al. (2011) for quasi-uniform grids, to variable-resolution grids. The success in Chen et al. (2011) relies on the crucial fact that the grid resolution is accounted for in the new formulation (see (27) in Section 2). The grid-resolution dependent factor in (27) enables the closure to adjust itself as the grid resolution changes. More specifically, it effects more dissipation as the grid coarsens, in a nonlinear fashion according to (27). This is expected as, in general, more eddies are under-resolved on a coarser grid. Since the grid resolution has been accounted for, it seems natural to ask, with this new formulation, whether the APVM closure can act across different scales present on a multi-resolution grid. The answer to this question can not a priori be derived from the results on quasi-uniform grids, because the

non-uniformity in grid resolution present in multi-resolution grids may cause complications such as the deterioration of accuracy in the solutions and/or the hindering of waves from one resolution zone to another. In Ringler et al., the multi-resolution approach is explored. A suite of multi-resolution grids which have smooth transitions between fine and coarse regions are used. As expected from hyperbolic systems, the overall accuracy is controlled by the coarsest mesh resolution. So while including regions of mesh refinement did not lead to reductions in global error norms, such regions of refinement will allow for the emergence of phenomena (such as mesoscale ocean eddies) that can not exist in coarse-mesh regions. Based on this finding, here we numerically explore how well the APVM with the new formulation developed in Chen et al. (2011) acts across the wide range of scales present in a multi-resolution grid, using a subset of the same suite of multi-resolution grids used in Ringler et al.. In the somewhat idealized setting of our numerical exploration, the issue related to traveling waves is not significant because of the smooth transition between fine and coarse regions. Nevertheless, we acknowledge that, in more realistic situations, this issue will need to be carefully addressed.

Without delving into details (see Section 3 instead), we shall briefly describe the numerical approach that we adopt in this work towards the question raised above. A series of simulations are conducted, with both the original and new formulations of the APVM, on each of the grids selected for this study. A simple optimization technique is applied to determine the optimal parameters on each grid for both formulations of the APVM. We evaluate the scale-aware property of the new formulation by comparing the range of optimal parameters for the new and the original formulations, their performances with the numerically identified optimal parameters on a specific grid, and their insensitivity near the optimal parameters. From these results, we are able to draw a positive answer to the above question.

2. The scale-aware anticipated potential vorticity method

In this section we briefly recall the scale-aware formulation of the APVM developed in Chen et al. (2011), and the main steps of the scale analysis that leads to the formulation. Full details of the analysis, for both the two-dimensional Euler equations and the shallow water equations, are given in Chen et al. (2011). In this work, we focus on the shallow water system only.

The APVM closure for the system of the one-layer shallow-water equations can be written as

$$\begin{cases} \dfrac{\partial h}{\partial t} + \nabla \cdot (h\mathbf{u}) = 0, \\ \dfrac{\partial \mathbf{u}}{\partial t} + (q - D)\mathbf{k} \times h\mathbf{u} = -\nabla(gh + K), \end{cases} \tag{4}$$

where h denotes the fluid thickness and $K = |\mathbf{u}|^2/2$ the kinetic energy. For shallow-water flows, the potential vorticity is defined as the ratio between the absolute vorticity and the fluid thickness, i.e.,

$$q = \frac{\eta}{h} \tag{5}$$

with the absolute vorticity η given by

$$\eta = \zeta + f \tag{6}$$

and the relative vorticity ζ given by

$$\zeta = \mathbf{k} \cdot \nabla \times \mathbf{u}. \tag{7}$$

The term D is the APVM correction to the potential vorticity. Taking the curl of the second equation of (4) and using (7), we obtain

$$\frac{\partial \eta}{\partial t} + \nabla \cdot ((q - D)h\mathbf{u}) = 0. \tag{8}$$

Replacing η by hq in (8) and using the first equation of (4) for the height h, we infer that

$$h\left(\frac{\partial q}{\partial t} + \mathbf{u} \cdot \nabla q\right) = \nabla \cdot (Dh\mathbf{u}). \tag{9}$$

Multiplying (9) by q, we obtain

$$h\frac{\partial}{\partial t}\left(\frac{1}{2}q^2\right) + h\mathbf{u}\cdot\nabla\frac{q^2}{2} = q\nabla\cdot(Dh\mathbf{u}). \tag{10}$$

Multiplying the first equation of (4) by $q^2/2$, we obtain

$$\frac{q^2}{2}\frac{\partial h}{\partial t} + \frac{q^2}{2}\nabla\cdot(h\mathbf{u}) = 0. \tag{11}$$

Combining (10) and (11), we have

$$\frac{\partial}{\partial t}\left(\frac{1}{2}hq^2\right) + \nabla\cdot\left(\frac{1}{2}hq^2\mathbf{u}\right) = q\nabla\cdot(Dh\mathbf{u}). \tag{12}$$

Let $\mathcal{M}$ denote the spatial domain. If $\mathcal{M}$ is bounded, then the non-penetration boundary condition is assumed on the boundary, i.e., $\mathbf{u}\cdot\mathbf{n} = 0$, $\mathbf{n}$ being the outward normal vector on the boundary $\partial\mathcal{M}$. If $\mathcal{M}$ is the whole sphere, then no boundary conditions are needed. Integrating (12) over $\mathcal{M}$, we obtain the potential enstrophy balance equation

$$\frac{\mathrm{d}}{\mathrm{d}t}\int_{\mathcal{M}}\frac{1}{2}hq^2 = -\int_{\mathcal{M}} Dh\mathbf{u}\cdot\nabla q. \tag{13}$$

It is easy to see that, if the correction term D is taken as

$$D = \gamma\mathbf{u}\cdot\nabla q, \tag{14}$$

then the right-hand side of (13) is negative. Indeed, with this choice of D, (13) becomes

$$\frac{\mathrm{d}}{\mathrm{d}t}\int_{\mathcal{M}}\frac{1}{2}hq^2 = -\int_{\mathcal{M}}\gamma h\left|\mathbf{u}\cdot\nabla q\right|^2. \tag{15}$$

Because the flow is predominantly two dimensional and the variations in h are small compared to h itself, we assume that h on both sides of (15) is constant. Then, that equation reduces to

$$\frac{\mathrm{d}}{\mathrm{d}t}\int_{\mathcal{M}}\frac{1}{2}q^2 = -\int_{\mathcal{M}}\gamma\left|\mathbf{u}\cdot\nabla q\right|^2. \tag{16}$$

Let ℓ denote the grid scale and χ_ℓ denote the enstrophy dissipation rate at the scale ℓ. Noticing the relations $t_\ell \sim \ell/u_\ell$ and $u_\ell \sim \psi_\ell/\ell$, we derive from the left-hand side of (16) that

$$\chi_\ell \sim \frac{q_\ell^2}{t_\ell} \sim \frac{\psi_\ell q_\ell^2}{\ell^2}, \tag{17}$$

where q_ℓ and ψ_ℓ are the potential vorticity and streamfunction, respectively, at the scale ℓ and the symbol "$\sim$" means "equal within an order one constant." From the right-hand side of (16), we infer that

$$\chi_\ell \sim \gamma |u_0 \nabla q_\ell|^2 \sim \gamma \overline{ke} \frac{q_\ell^2}{\ell^2}. \tag{18}$$

In the above, we have replaced $\mathbf{u}$ by u_0, the magnitude of the zeroth mode of the velocity field, based on the conjecture that the term $|u_0 \nabla q_\ell|^2$ dominates in all contributions to the potential enstrophy dissipation at the scale ℓ. This conjecture is reached through a delicate analysis of the nonlinear interaction between motions of different scales, and is supported by the extensive numerical results in Chen et al. (2011). The homogeneity in mesh resolution is not essential for the conclusion of this conjecture, and we expect that it remains valid on variable-resolution grids. Comparing (17) and (18), we obtain

$$\gamma \sim \overline{ke}^{-1} \psi_\ell. \tag{19}$$

Using again the relation $u_\ell \sim \psi_\ell / \ell$, we can rewrite (19) as

$$\gamma \sim \overline{ke}^{-1} u_\ell \ell. \tag{20}$$

We remark that (20) has the dimension of time which is consistent with the original choice of $\sigma \, \mathrm{d}t$ as the form of γ; see (3).

The expression (19) is not of use in practice because ψ_ℓ is not readily available. As usual (see, e.g., Berselli et al. (2006)), this difficulty can be circumvented by equating χ_ℓ to the overall model potential enstrophy dissipation rate χ. To do so, we first need to determine the relation between q_ℓ and ψ_ℓ. According to (5)–(7), the potential vorticity q is defined as

$$q = \frac{\mathbf{k} \cdot \nabla \times \mathbf{u} + f}{h}. \tag{21}$$

We note that variations in the Coriolis parameter f are unimportant at the grid scale ℓ. On the other hand, we continue to use the assumption that the variation in h is small compared to h itself and replace h in the above equation by its mean value $\overline{h}$. Hence, we have

$$q_\ell \sim \frac{\psi_\ell}{\ell^2 \overline{h}}. \tag{22}$$

With (22), the potential enstrophy dissipation rate χ_ℓ in (17) takes the form

$$\chi_\ell \sim \frac{\psi_\ell^3}{\ell^6 \overline{h}^2}. \tag{23}$$

Using this new form for χ_ℓ, we can infer from (19) that

$$\gamma \sim \overline{ke}^{-1} \chi_\ell^{\frac{1}{3}} \ell^2 \overline{h}^{\frac{2}{3}}. \tag{24}$$

Note that the overall model enstrophy dissipation rate is given by

$$\chi = \gamma |\mathbf{u} \cdot \nabla q|^2. \tag{25}$$

Replacing χ_ℓ in (24) by χ and using (25), we have

$$\gamma \sim \overline{ke}^{-\frac{3}{2}} |\mathbf{u} \cdot \nabla q| \overline{h} \ell^3. \tag{26}$$

The full form for γ is then given by

$$\gamma = \alpha \overline{ke}^{-\frac{3}{2}} |\mathbf{u} \cdot \nabla q| \overline{h} \ell^3, \tag{27}$$

where α is a constant independent of the scale and state of the flow. We remark that the average kinetic energy $\overline{ke}$, the advection of the potential vorticity $\mathbf{u} \cdot \nabla q$, and the average height $\overline{h}$ can all be computed from the corresponding dynamical variables of the model. The grid scale ℓ can be represented by the distance between two neighboring grid points. Thus, α is the only parameter in the expression (27) for γ and will be studied in detail in the next section.

3. Numerical results and analysis

The purpose of this work is to evaluate the scale-aware property of the new APVM formulation on variable-resolution grids. Roughly speaking, we want to find out whether the optimal parameter is invariant in different grid settings, or how it responds to changes in grid settings. Before we can conduct such studies, we first need to address the question of how the optimal parameter can be determined on a specific grid setting. This is explained in the Section a. The numerical results and their analysis are then presented in Section b.

a. Preliminaries

As with the evaluation of most closures, the measure of effectiveness is based on the ability of a low-resolution simulation with the closure to reproduce certain important aspects of a high-resolution, reference simulation. In the simulations below, we evaluate the closure based in its ability to reproduce the spectrum of the potential enstrophy (PE) obtained in the high-resolution simulation.

It has been conjectured (see, e.g., Batchelor (1969); Kraichnan (1967)) and approximately verified in the literature (see, e.g., Lilly (1969, 1971)) that for two-dimensional incompressible turbulent flows, the spectrum of the enstrophy satisfies a -1 power law. Equivalently, the spectrum of the kinetic energy satisfies a -3 power law, in contrast to the famous $-5/3$ power law for three-dimensional turbulent flows (Frisch 1995; Kolmogorov 1941a,b). Our reference solution is computed on a very fine grid, with the least damping that is still capable of producing a potential enstrophy spectrum that approximates the -1 power law well. The damping mechanism used to produce the reference solution is provided by conventional hyperviscosity that has been widely used in geophysical fluid dynamics.

To study the spectra of the fluids on the whole sphere, the natural choice of basis functions are the spherical harmonic functions (Adams and Swarztrauber 1997). The properties of the spherical harmonics have been briefly recalled in Chen et al. (2011).

We have chosen to evaluate the effectiveness of the closure based on its ability to reproduce the potential enstrophy spectra of the reference solution. Hence we define the "error" in an approximate solution as the mean distance between the PE spectrum curves, within the inertial range, of the approximate solution and the high-resolution reference solution. More specifically, let P (resp. P_r) denote the spectral density function for the PE of the approximate (resp. reference) solution. Then the error between the approximate and the reference solutions is defined as

$$d = \frac{1}{k_1 - k_0 + 1} \sum_{k=k_0}^{k_1} |\log \widehat{P}(k) - \log \widehat{P}_r(k)|, \tag{28}$$

where k denotes the spherical wavenumber, and k_0 and k_1 are the starting and ending wavenumbers for the subrange.

b. Comparison and analysis of the numerical results

We conduct numerical experiments with the standard shallow water test case #5, which involves an initially zonal flow impinging on a mountain topography. The initial zonal velocity u of the flow and the surface height $\widetilde{h}$ are given by

$$u = u_0 \cos\theta,$$
$$g\widetilde{h} = gh_0 - \left(a\Omega u_0 + \frac{u_0^2}{2}\right)\cos\theta,$$

respectively. The mountain, which is part of the lower boundary, has the form

$$b = b_0\left(1 - \frac{r}{R_0}\right).$$

The fluid thickness h is then given by

$$h = \widetilde{h} - b.$$

In the above, θ represents the latitude as usual, and the other physical parameters are set following Williamson et al. (1992), namely, $\Omega = 7.292 \times 10^{-5}\mathrm{s}^{-1}$, $g = 9.80616\mathrm{m\,s}^{-2}$, $a = 6.37122 \times 10^6\mathrm{m}$, $u_0 = 20\mathrm{m\,s}^{-1}$, $h_0 = 5960\mathrm{m}$, $b_0 = 2000\mathrm{m}$, $R_0 = \pi/9$, $r^2 = \min[R_0^2, (\lambda - \lambda_c)^2 + (\theta - \theta_c)^2]$, with λ being the longitude, and $\lambda_c = -\pi/2$, $\theta_c = \pi/6$. Thus the mountain is confined to a 20° region surrounding the center ($\lambda_c = -\pi/2$, $\theta_c = \pi/6$) of the mountain. We remark that the topography is not a source or sink of potential vorticity, but instead acts as an inhomogeneity that leads to the breakdown of the nonlinearly-balanced geostrophic zonal jet. There is no other external forces added, and therefore this is a slowly decaying turbulent flow.

The reference solution is computed on an SCVT mesh with 655362 cells ($dx \approx 30\,\mathrm{km}$), with the traditional ∇^4 dissipation of $10^9\,\mathrm{m}^4\,\mathrm{s}^{-1}$. The shallow-water test case #5 evolves

into turbulence in about 20 to 25 days. A snapshot of the potential vorticity field on day 50 is shown in Figure 1. The axis of the globe is slightly tilted in order to better display the structure of the potential vorticity field on the northern hemisphere. We plot the spectrum of the potential enstrophy of the reference solution on day 150 in Figure 2. An inertial range of width approximately one decade appears between wave numbers 20 and 120, which approximately verifies the -1 power law for potential enstrophy spectra.

Approximate solutions are computed on variable-resolution grids refined in a region including the mountain topography. More specifically, the grids are refined in the area 30° surrounding the center of the mountain topography, and smoothly coarsen outside this region. One set of grids have 40962 cells, with the contrast ratio between the finest and coarsest grid resolutions ranging over {1, 2, 4, 8, 16}. Another set of grids have 163842 cells, with the contrast ratio ranging over {1, 2}. More details and visual plots of these grids are available in Ringler et al.. For our purpose, we list the resolutions of the fine and coarse regions of the aforementioned grids in Table 1. In what follows, these grids will be referred to as the 40962-cell X1 grid etc. We note that the mid-latitude Rossby radius in the simulations is approximately 2000km. The coarsest region in these meshes has a resolution of 592km. Thus, in all simulations the Rossby radius is resolved. We also note that the finest region on these meshes has a resolution of 37km, which is at the same level as the resolution (30km) of the uniform high-resolution grid used for the reference solution.

On each of the grids mentioned above, a series of simulations with the original formulation (3) and the new formulation (27) of the APVM are conducted. The parameter σ of the original formulation assumes values starting from zero and increases by 0.002 each time; the parameter α of the new formulation starts from zero, and increases by 0.0001 each time. The increments in the sampling values of the parameters for both formulations are determined empirically so that a good sample is obtained with around 100 simulations, except for the extreme case of the original APVM on the 40962 X16 grid, which requires 300 simulations! The fine-resolution zones on the grids demand small time steps according to

the CFL criteria (Courant et al. 1967). The time step (see Table 2) used for each of the grid in our simulations is determined empirically so that stable solutions are achieved. In Chen et al. (2011), a strict invariance of the optimal parameter of the new formulation with respect to the time step size is demonstrated. The explanation is that the model incorporating the new APVM formulation consists of partial differential equations that are independent of the time step size (cf. the original formulation (3)), and therefore the solutions of the model are independent of the time step size as well. This argument applies in the multi-resolution setting as well, and therefore the invariance of the optimal parameter of the new formulation with respect to the time step size is assumed, and will not be explicitly addressed in this work. We note that, on each grid, the same time step is used for both the original and new APVM formulations. Hence, the following comparisons between the results of these two formulations are sensible.

For each simulation, the error in the approximate solution compared to the high-resolution reference solution is computed using (28). The errors for the original APVM formulation, on all the aforementioned grids, are plotted against the original APVM parameter σ in Figure 3. The error curve for the 40962 X16 grid is truncated on this plot. The high contrast ratio between the fine and coarse resolutions on this grid demands a much wider parameter interval in order to reveal the optimal parameter. The whole error curve on this grid, obtained on an interval of [0, 0.60], continues to decrease beyond $\sigma = 0.20$, flattens and reaches its minimum at $\sigma = 0.408$, and then rises up again. The errors for the new APVM formulation, on all the aforementioned grids, are plotted in Figure 4 against the new APVM parameter α. The optimal parameters for the new and original formulations of the APVM, on each of the grids used for this study, are listed in Table 3. It is seen that the optimal parameter for the original formulation ranges from 0.004 to 0.408, with a factor of 100 change! The optimal parameter for the new formulation ranges from 0.0008 to 0.0033, with a factor of 4 change. On variable-resolution grids, it is not possible to correlate the optimal parameter to the grid resolutions, as we did in Chen et al. (2011). It is because, on each grid, there

are generally a wide range of grid scales present. However, the fact that the range for the values of the optimal parameter of the new formulation is much narrower than that for the original formulation is the first indicator that the new APVM formulation is able to act appropriately across scales, i.e., it is scale-aware.

The scale-aware property of the new formulation is also demonstrated by the fact that, on all the grids used for this study, the new formulation produces minima that are at least as low as those produced by the original formulation. In certain situations, e.g. on the 40962-cell X8 and the 40962-cell X16 grids, it actually produce lower minima, thanks to its ability to act appropriately across the vast range of scales present on these grids.

The 40962-cell X16 grid causes a surge in the value of the optimal parameter for the original formulation (Table 3). A detailed look at the spectrum curves produced with various parameter values reveals why this happens, and also demonstrates more clearly the strength of the scale-aware feature of the new formulation. In Figure 5, we plot the PE spectrum curves with $\sigma = 0.100$, 0.200, 0.300, 0.400, 0.500, and 0.600 for the original formulation of the APVM. At $\sigma = 0.100$, which is already larger than the optimal parameter of the original formulation on any other grid, the spectrum curve stays way above the reference spectrum curve. Its straying behavior near wave number 10 reveals that the mesoscale motions of the flow are corrupted, apparently due to the lack of dissipation in the coarse region of the mesh. Larger values are needed for the parameter σ to ensure proper dissipation in the coarse region. When the parameter has been raised to levels ($\sigma = 0.400$, 0.500, 0.600) for which the spectrum curves near wave number 10 match the reference spectrum curve reasonably well, the curves at high wavenumbers suffer from over-dissipation in the fine regions. It is clear that the conflicting needs of dissipation in the coarse and fine regions on the mesh makes it very challenging to bring the PE spectrum curve of the approximate solution evenly close to that of the reference solution. In Figure 6 we plot the PE spectrum curves produced with $\alpha = 0.0010$, 0.0020, 0.0030, 0.0040, and 0.0050 for the APVM in the new formulation. Starting from $\alpha = 0.0010$, as the parameter increases, the spectrum curve

comes down at both low (10) and high (100) wave numbers, demonstrating that the new formulation maintains control at both the low and high wave numbers equally well. It can be seen that, at $\alpha = 0.0030$, the spectrum curve of the approximate solution is close to the reference spectrum curve across the inertial range. As Table 3 shows, the optimal value for α on the 40962-cell X16 grid is 0.0033.

As the foregoing results and analysis have shown, the new APVM formulation is able to act appropriately across grid scales, and produces better results compared to the original formulation, in situations where a vast range of scales are present. The results have also shown that the parameter of the new formulation is not strictly scale invariant, because it varies, albeit with a relatively small factor of change. Hence, it is crucial to assess the robustness or the insensitivity of the APVM with the new formulation with respect to the parameter values near the numerically identified optimal values. On all but the 40962-cell X8 and 40962-cell X16 grids, the error curves (see Figures 3 and 4) produced by the original formulation and the new formulation find their minimizers roughly in the first quarter of the whole intervals. Thus the sampling intervals for the original formulation ([0, 0.200]) and for the new formulation ([0, 0.0100]) are comparable, and it makes sense to compare the "flatness" near the minimizers, which is an indicator of the insensitivity of the results to the parameters. The minimizers on the 40962-cell X8 and 40962-cell X16 grids fall in different quarters of the respective whole intervals (Figure 3), and thus are not suitable for this comparison. Comparing Figures 3 and 4, we see that generally the curves produced by the new formulation are "flatter" near the minimizer, indicating that the results are less sensitive to the changes in the parameter α. This lends us confidence that, for the new formulation, once an optimal parameter determined on a specific grid, it can be safely used on other grids, and should produce reasonably good results. To demonstrate this, we pick $\alpha = 0.0020$, a representative value in the range $[0.0011, 0.0032]$ found before for the optimal parameter of the new formulation, and plot, in Figure 7, the spectrum curves produced with this value of the parameter, on all the grids used for this study. We see that the curves from

the 40962-cell X1, 40962-cell X2, 40962-cell X4, 163842-cell X1, and 163842-cell X2 grids match very well with the reference spectrum curve. The 40962-cell X8 and 40962-cell X16 grids are known to be challenging for numerical simulations due to the presence of a vast range of scales. Even so, the spectrum curves produced with the representative parameter value on these two grids stay reasonably close to the reference spectrum curve. Lastly, we note that the chosen optimal parameter $\alpha = 0.0020$ here is consistent with the optimal interval found in Chen et al. (2011) for the new APVM formulation on quasi-uniform grids.

4. Conclusions

In this work, we numerically evaluate the scale-aware property of a new formulation of the APVM on multi-resolution grids. Numerical simulations are conducted on a sample set of variable-resolution SCVT grids, using the MPAS computational framework. Comparison is made between the new formulation and the original formulation, which has been used in earlier literatures. The scale-aware property of the new formulation is demonstrated by the facts that (i) the range for the optimal parameter of the new formulation is much narrower than that for the original formulation; (ii) on grids that are challenging for numerical simulations due to the high contrast ratios between fine and coarse resolutions, the new APVM formulation produces lower minima at the identified optimal parameters; (iii) the APVM closure with the new formulation is less sensitive to the parameter near the numerically identified optimal values. The last point is important as it shows that one parameter identified for a certain grid can be safely used on other grids.

This work and Chen et al. (2011) are part of an on-going effort to generalize subgrid eddy parametrization schemes to variable-resolution grids. Our success with the APVM demonstrates that matching spectra is a viable approach towards deriving scale-aware subgrid closures. Though admittedly, when dealing with more complex parametrization schemes, e.g. the Gent-McWilliams eddy closure, some simplifying assumptions that are valid in the case of shallow water flows will have to be carefully re-evaluated. We would like to remark on two of such issues before we finish.

The closure presented in this work includes the assumption of small variations in fluid thickness. Namely, we assume that variations in the fluid thickness h are small compared to the mean fluid thickness $\bar{h}$, and then proceed to replace h by $\bar{h}$ in (15) and (21). For a broad class of shallow-water systems where this closure might be utilized, this will, in general, be a valid assumption. However, as we apply the closure to more realistic systems, such as the isopycnal model of the ocean circulation (see, e.g., Ringler and Gent (2010)), this assumption will have to be carefully reevaluated.

The scale-aware formulation presented in Chen et al. (2011) and the current work is derived based on another crucial assumption, namely the isotropy of the flow. Even though this assumption is approximately true for many cases, it is conceivable that, in order to faithfully represent a realistic geophysical flow, non-isotropic features of the flow will need to be taken into account. For example, the wave-turbulence interactions (see, e.g., Pedlosky (1987); Rhines (1975)) have profound influence on the long-term behavior of the global oceanic and atmospheric circulations, and should be considered in designing subgrid closures aimed for these flows.

Acknowledgments.

Q. Chen and M. Gunzburger were supported by the US Department of Energy grant number DE-SC0002624 as part of the *Climate Modeling: Simulating Climate at Regional Scale* program. T. Ringler was supported by the DOE Office of Science's Climate Change Prediction Program DOE 07SCPF152.

REFERENCES

Adams, J. C. and P. N. Swarztrauber, 1997: Spherepack 2.0: A model development facility. *NCAR Technical Note NCAR/TN-436-STR*.

Arakawa, A. and W. Schubert, 1974: Interaction of a cumulus cloud ensemble with the large-scale environment, part i. *Journal of the Atmospheric Sciences*, **31 (3)**, 674–701.

Batchelor, G. K., 1969: Computation of the energy spectrum in homogeneous two-dimensional turbulence. *Physics of Fluids*, **12 (12)**, II–233–II–239.

Berselli, L. C., T. Iliescu, and W. J. Layton, 2006: *Mathematics of large eddy simulation of turbulent flows*. Scientific Computation, Springer-Verlag, Berlin, xviii+348 pp.

Chen, Q., M. Gunzburger, and T. Ringler, 2011: A scale-invariant formulation of the anticipated potential vorticity method. *Monthly Weather Review*, **139 (8)**, 2614–2629, doi: 10.1175/MWR-D-10-05004.1.

Chen, Q. and M. Gunzburger, ????: Goal-oriented a posteriori error estimation for finite volume methods. Submitted.

Courant, R., K. Friedrichs, and H. Lewy, 1967: On the partial difference equations of mathematical physics. *IBM J. Res. Develop.*, **11**, 215–234.

Du, Q., V. Faber, and M. Gunzburger, 1999: Centroidal Voronoi tessellations: applications and algorithms. *SIAM Rev.*, **41 (4)**, 637–676 (electronic).

Du, Q., M. Gunzburger, and L. Ju, 2003: Constrained centroidal voronoi tessellations for surfaces. *SIAM Journal on Scientific Computing*, **24 (5)**, 1488–1506.

Frisch, U., 1995: *Turbulence: the legacy of AN Kolmogorov*. Cambridge Univ Pr.

Gent, P. R. and J. C. McWilliams, 1990: Isopycnal mixing in ocean circulation models. *Journal of Physical Oceanography*, **20 (1)**, 150–155, doi:10.1175/1520-0485(1990)020⟨0150:IMIOCM⟩2.0.CO;2.

Kolmogorov, A. N., 1941a: Dissipation of energy in locally isotropic turbulence. *Proceedings of the USSR Academy of Sciences*, **32**, 16–18.

Kolmogorov, A. N., 1941b: The local structure of turbulence in incompressible viscous fluid for very large reynolds numbers. *Proceedings of the USSR Academy of Sciences*, **30**, 299–303.

Kraichnan, R. H., 1967: Inertial ranges in two-dimensional turbulence. *Physics of Fluids*, **10 (7)**, 1417–1423.

Lilly, D. K., 1969: Numerical simulation of two-dimensional turbulence. *Physics of Fluids*, **12 (12)**, II–240–II–249.

Lilly, D. K., 1971: Numerical simulation of developing and decaying two-dimensional turbulence. *Journal of Fluid Mechanics*, **45 (02)**, 395–415, `http://journals.cambridge.org/article_S0022112071000107`.

Pedlosky, J., 1987: *Geophysical fluid dynamics, 2nd edition*. Springer, xiv+710 pp. pp.

Rhines, P. B., 1975: Waves and turbulence on a beta-plane. *Journal of Fluid Mechanics*, **69 (03)**, 417–443.

Ringler, T. D., D. Jacobsen, M. Gunzburger, L. Ju, M. Duda, and W. Skamarock, ????: Exploring a multi-resolution modeling approach within the shallow-water equations. Revised.

Ringler, T. D., J. Thuburn, J. B. Klemp, and W. C. Skamarock, 2010: A unified approach to energy conservation and potential vorticity dynamics for arbitrarily-structured c-grids. *J. Comput. Phys.*, **229 (9)**, 3065–3090.

Ringler, T. and P. Gent, 2010: An eddy closure for potential vorticity. *Ocean Modelling*, submitted.

Ringler, T., L. Ju, and M. Gunzburger, 2008: A multiresolution method for climate system modeling: application of spherical centroidal voronoi tessellations. *Ocean Dynamics*, **58**, 475–498, URL `http://dx.doi.org/10.1007/s10236-008-0157-2`, 10.1007/s10236-008-0157-2.

Sadourny, R. and C. Basdevant, 1985: Parameterization of subgrid scale barotropic and baroclinic eddies in quasi-geostrophic models: Anticipated potential vorticity method. *Journal of the Atmospheric Sciences*, **42 (13)**, 1353–1363, doi:10.1175/1520-0469(1985)042⟨1353:POSSBA⟩2.0.CO;2.

Williamson, D. L., J. B. Drake, J. J. Hack, R. Jakob, and P. N. Swarztrauber, 1992: A standard test set for numerical approximations to the shallow water equations in spherical geometry. *Journal of Computational Physics*, **102 (1)**, 211 – 224.

List of Tables

TABLE 1. Grid resolutions in kilometers. In each parenthesis, the first number is the finest grid resolution, and the second number is the coarsest grid resolution on the particular grid.

No. grid points	X1	X2	X4	X8	X16
40962	(120, 120)	(65, 130)	(48, 190)	(39, 310)	(37, 592)
163842	(60, 60)	(33, 65)			

TABLE 2. Time step size for simulations with both the original and new APVM formulations, in seconds.

Grid	Time step
40962-cell X1	172.8
40962-cell X2	172.8
40962-cell X4	172.8
40962-cell X8	86.4
40962-cell X16	43.2
163842-cell X1	172.8
163842-cell X2	86.4

TABLE 3. Optimizing parameters.

Grid	Original	New
40962-cell X1	0.018	0.0018
40962-cell X2	0.018	0.0018
40962-cell X4	0.024	0.0024
40962-cell X8	0.074	0.0026
40962-cell X16	0.408	0.0033
163842-cell X1	0.004	0.0008
163842-cell X2	0.008	0.0012

List of Figures

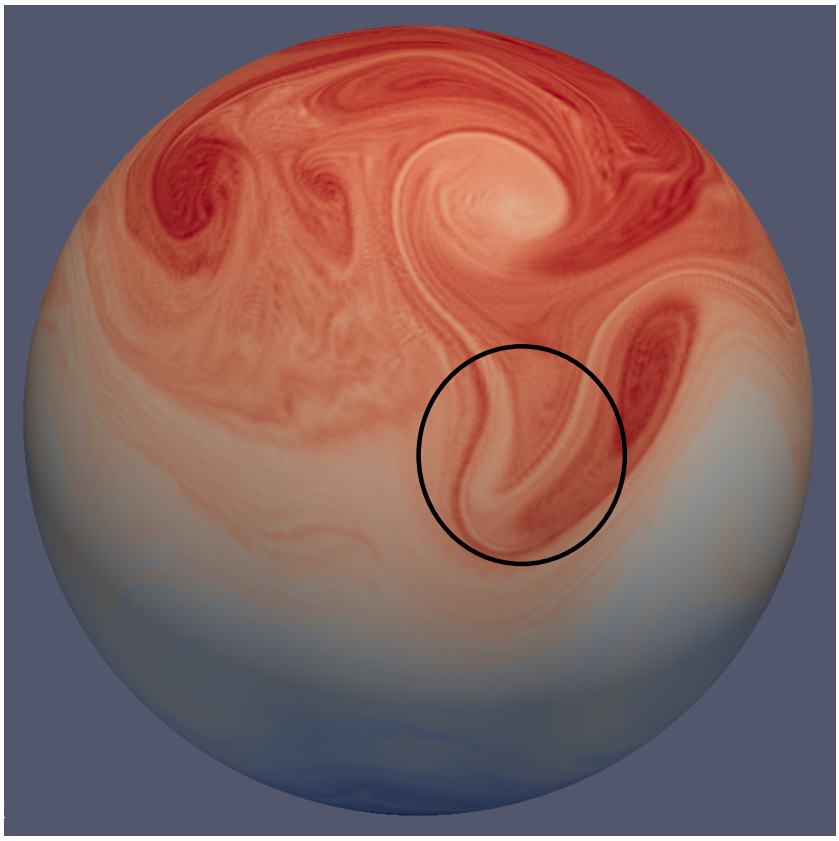

FIG. 1. The potential vorticity field on day 50, with values in the range from $-3.2 \times 10^{-8}\mathrm{m}^{-1}\mathrm{s}^{-1}$ to $3.2 \times 10^{-8}\mathrm{m}^{-1}\mathrm{s}^{-1}$. The location of the mountain is indicated by the circle.

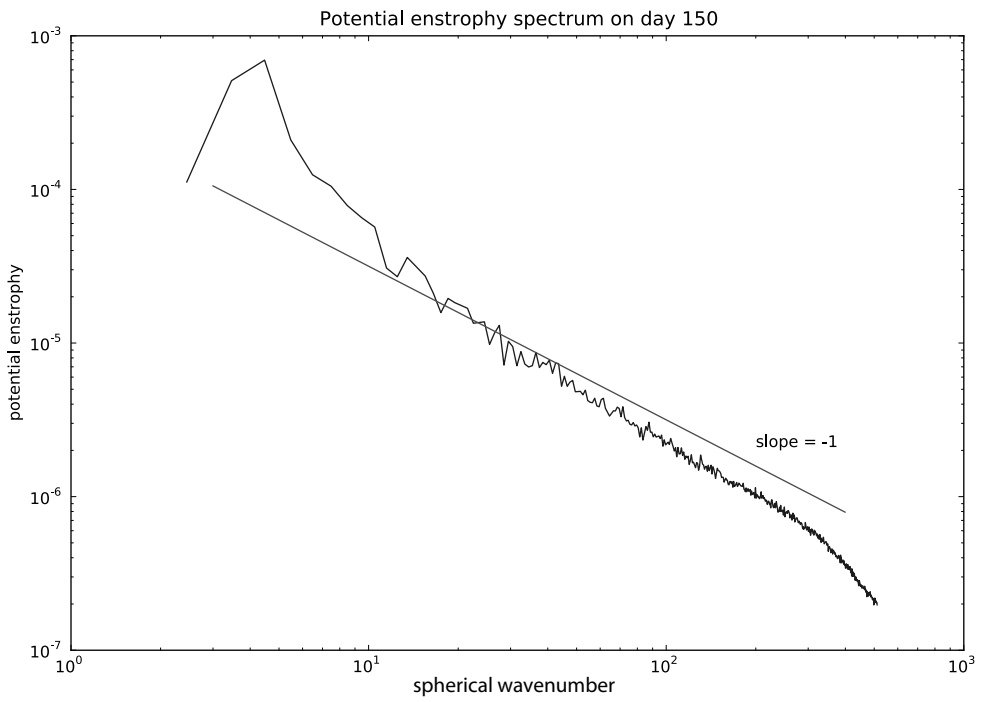

FIG. 2. The potential enstrophy spectrum on day 150 for the reference solution.

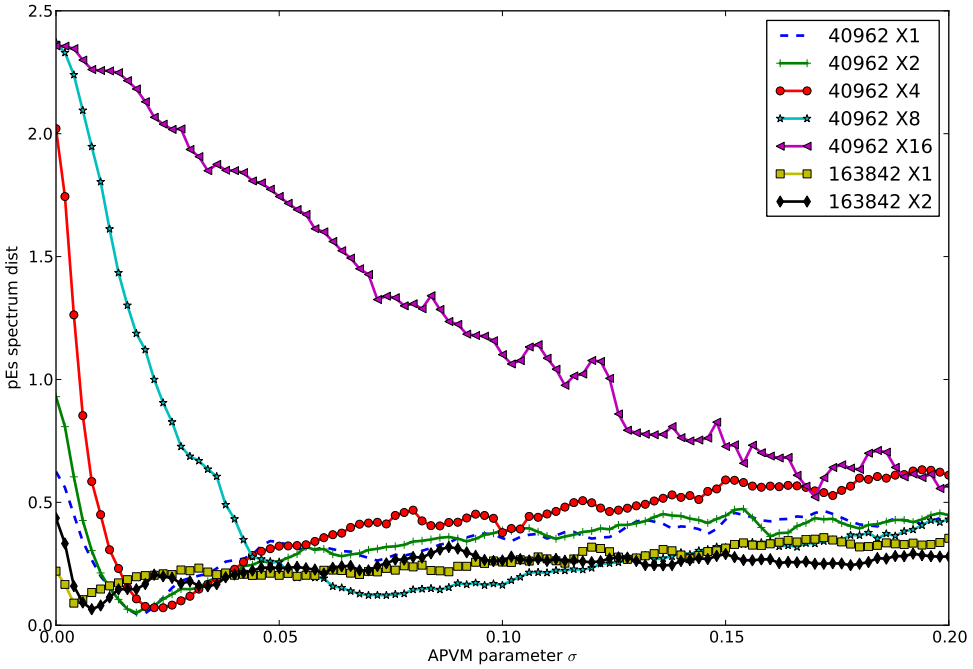

FIG. 3. Errors in the potential enstrophy spectrum, computed with the original formulation of the APVM on a series of variable-resolution grids.

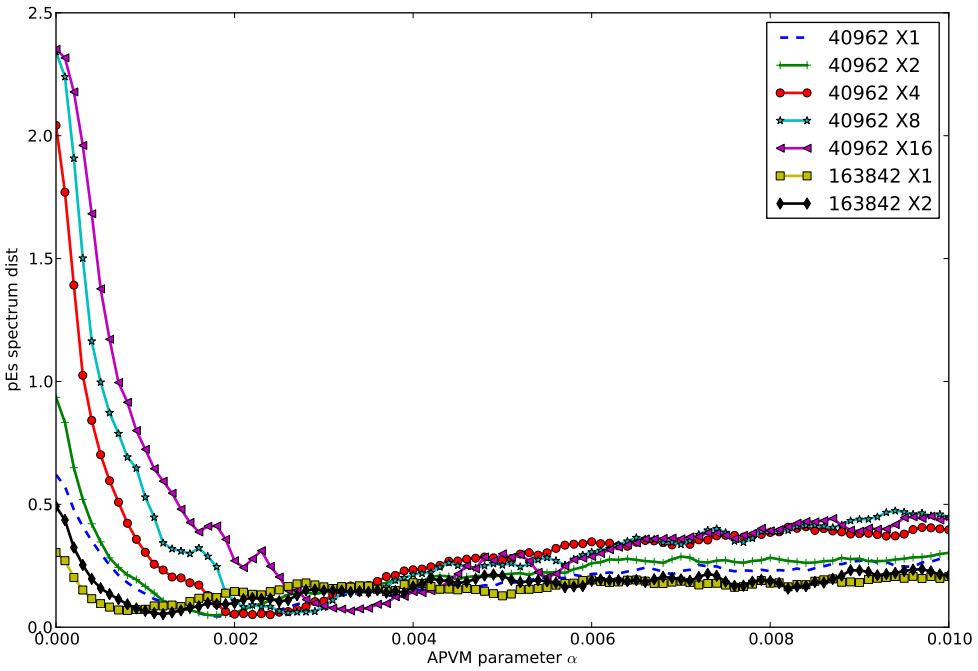

FIG. 4. Errors in the potential enstrophy spectrum, computed with the new formulation of the APVM on a series of variable-resolution grids.

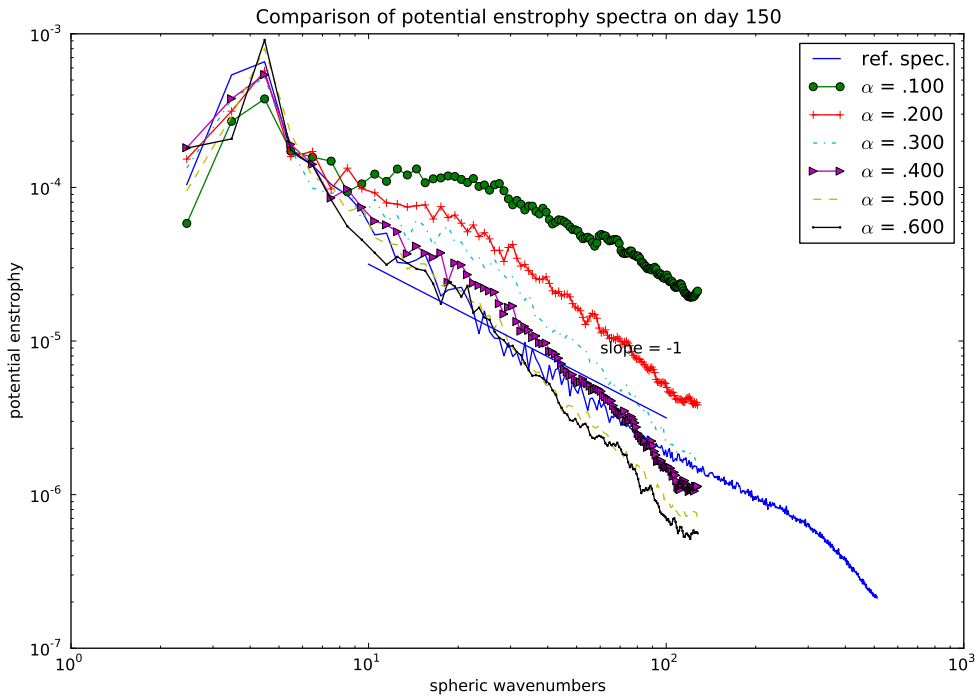

FIG. 5. Plots of spectrum curves with the APVM parameter $\sigma = 0.1, 0.2, 0.3, 0.4, 0.5, 0.6$. The simulations are conducted with the APVM in its original formulation and on the 40962-cell x16 variable-resolution grid.

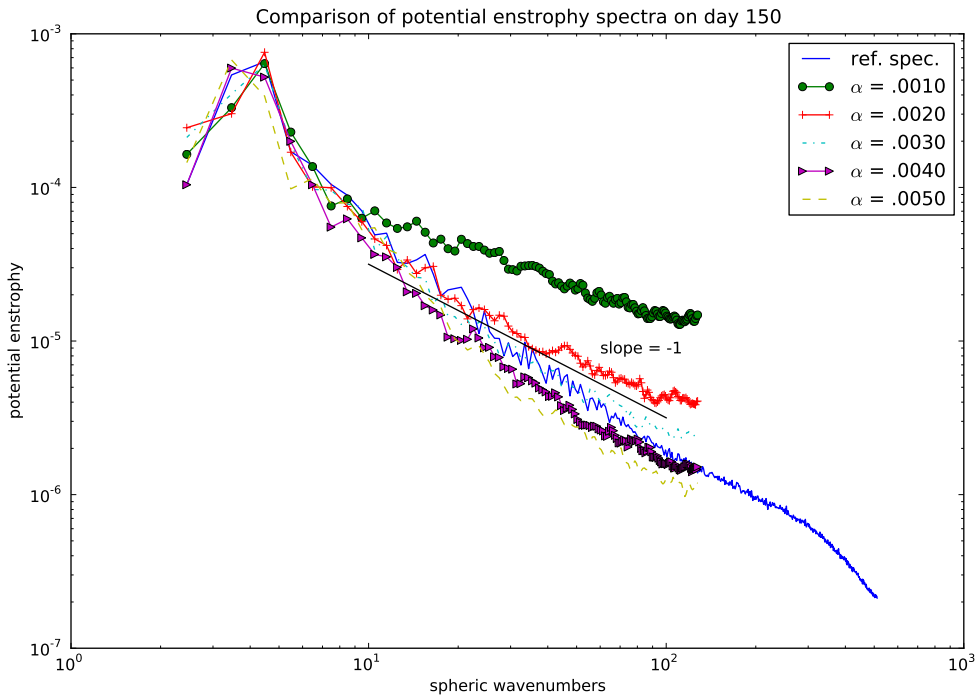

FIG. 6. Plots of the potential enstrophy spectrum curve with APVM parameter α = .0010, .0020, .0030, .0040, .0050. The simulations are conducted with the APVM in the new formulation and on the 40962-cell x16 variable-resolution grid.

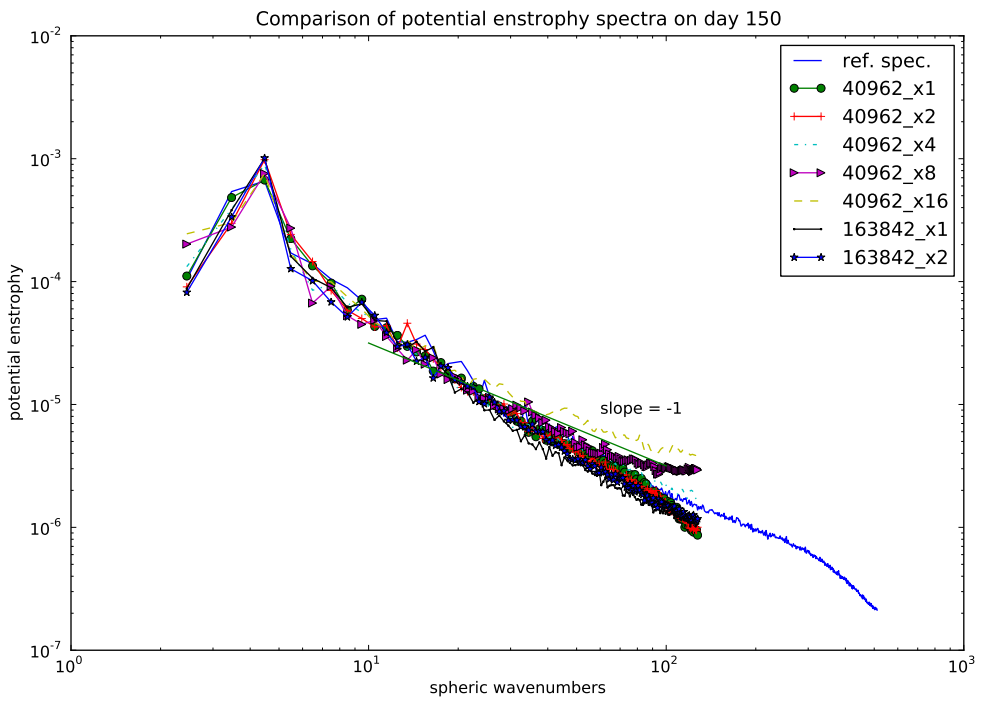

FIG. 7. Plots of the potential enstrophy spectrum on 40962-cell X2, 40962-cell X4, 40962 X8, 40962 X16, 163842 X1, and 163842 X2 variable resolution grids. The parameter α is taken as the mean (0.0020 for this plot) of the possible range $[0.0011, 0.0032]$.